arXiv:cond-mat/0507105v2 [cond-mat.supr-con] 18 Sep 2005

Crystal Symmetry, Electron-Phonon Coupling, and Superconducting Tendencies in Li_2Pd_3B and Li_2Pt_3B

K.-W. Lee and W. E. Pickett
Department of Physics, University of California, Davis, CA 95616, USA
(Dated: March 23, 2022)

After theoretical determination of the internal structural coordinates in Li_2Pd_3B, we calculate and analyze its electronic structure and obtain the frequencies of the two A_g phonons (40.6 meV for nearly pure Li mode, 13.0 meV for the strongly mixed Pd-Li mode). Pd can be ascribed a $4d^{10}$ configuration, but strong $4d$ character remains up to the Fermi level. Small regions of flat bands occur at -70 meV at both the Γ and X points. Comparison of the Fermi level density of states to the linear specific heat coefficient gives a dynamic mass enhancement of $\lambda = 0.75$. Rough Fermi surface averages of the deformation potentials $\mathcal{D}$ of individual Pd and Li displacements are obtained. While $\langle \mathcal{D}_{\rm Li} \rangle$ is small, $\langle \mathcal{D}_{\rm Pd} \rangle \approx 1.15$ eV/Å is sizable, and a plausible case exists for its superconductivity at 8 K being driven primarily by coupling to Pd vibrations. The larger d bandwidth in Li_2Pt_3B leads to important differences in the bands near the Fermi surface. The effect on the band structure of spin-orbit coupling plus lack of inversion is striking, and is much larger in the Pt compound.

PACS numbers: 74.70.Ad,71.20.Be,71.20.Dg

I. INTRODUCTION

The occurrence of superconductivity in compounds without inversion symmetry is an issue that has surfaced recently.[1] Although there seems to be very few compounds without a center of inversion which display robust superconductivity, a look at basic BCS theory reveals no severe obstruction to pairing, as long as there is no ferromagnetism, because time-reversal invariance (i.e., lack of magnetism) is sufficient to guarantee inversion symmetry in the Fermi surface ($\varepsilon_{-k\sigma}$=$\varepsilon_{k\sigma}$), therefore allowing zero momentum ($q = 0$) pairing. Ferromagnetism splits the spin (σ) degeneracy, restricting $q = 0$ pairing to triplet pairs. If inversion symmetry is lost, however, spin-orbit coupling (SOC) removes the spin degeneracy[2, 3] so that $q = 0$ pairing may be very sensitive to magnetism (including applied magnetic fields).[4, 5]

The lack of inversion symmetry has been suggested as a factor in the absence of superconductivity in MnSi[6, 7]; there are however other peculiar aspects of the space group (and resulting band structure)[8] that hamper elucidation of the effects of lack of inversion. Very recently a few examples of superconductivity in crystalline materials without inversion symmetry have been reported. $CePt_3Si$, with a crystal structure that is not close to any structure with inversion, has been found to be superconducting at $T_c = 0.75$ K.[1] The properties of this system are complicated due to its heavy fermion nature. SOC effects might be expected to cause complications[3] (due to the cerium) and the fact that superconductivity arises within the antiferromagnetic phase ($T_N = 2.2$ K) with enforced spin degeneracy may be relevant. Pressure induced superconductivity at $P_c = 2.6$ GPa and very low $T_c = 0.14$ K has been observed in UIr.[9] Electrons in UIr will experience strong SOC, however the crystal structure is only a small distortion away from one with inversion, so the effects of lack of inversion can only be determined by direct calculation.

Recently Li_2Pd_3B with a cubic but peculiar crystal structure without inversion symmetry has been discovered to be a $T_c = 8$ K superconductor by Togano and coworkers.[10, 11] It has an upper critical field $H_{c2} = 4$ T, and the Ginzburg-Landau parameter $\kappa = 21$, marking it as a strongly type-II superconductor.[11] Although there has been a suggestion[12] the superconductivity is dominated by strong electronic correlations related to three kinds of the Pd-Pd bond length,[13] experimental data is readily interpreted without any need for invoking correlation effects.[14, 15] Moreover, the density of states presented by Chandra *et al.* indicates that the Pd $4d$ bands are essentially completely filled,[16] leaving no reasonable expectation of correlation effects on the Pd site. The entire alloy system $Li_2B(Pd_{1-x}Pt_x)_3$ has been studied, and it was found[17] that T_c decreases almost linearly from 8 K (Pd end) to 2.8 K (Pt end). Since the volume is unchanged (the lattice constant of Li_2Pt_3B is 0.03% larger), the difference is due to (1) the slightly different chemistry of Pt, (2) the mass difference, or (3) the effect of stronger SOC combined with the lack of inversion symmetry of this lattice. Interpreted as an isotope shift $\alpha = -{\rm d}(\log T_c)/{\rm d}(\log M)$ leads to α greater than unity, although changes in both T_c and the mass M are too large for the differential definition of α to be realistic.

The Li_2Pd_3B structure has been described as a three-dimensionally distorted antiperovskite,[13]

characterized by strongly distorted corner-sharing BPd_6 octahedra. Thus on the local structural level Li_2Pd_3B appears to have similarity to $MgCNi_3$,[18] which is also an 8 K superconductor and has a similar valence balance (one more valence electron per formula unit). The lack of inversion symmetry is however only one aspect of the strong difference between the structures of Li_2Pd_3B and $MgCNi_3$. The structure and space group are discussed in some detail in Sec. II. There are several Pd and Pt based (anti)perovskite compounds[19] that may be more strongly related to Li_2Pd_3B, but they have not been studied nearly so thoroughly.

In this paper, we investigate in detail the electronic structure of Li_2Pd_3B and its relation to the local bonding and to the global symmetry of the crystal structure. We also begin some investigation into the lattice dynamics and electron-phonon coupling by studying the symmetric vibration of the Li and Pd atoms. We obtain rough estimates of the contribution of Li and Pd motions to electron-phonon coupling strength, and obtain a plausible case that Pd motion is the primary driver of superconductivity.

II. STRUCTURE AND CALCULATION METHOD

Our calculations were based on the experimentally reported structure[13] (cubic $P4_332$, No. 212), containing four formula units per primitive cubic cell, using the lattice constant 6.7436 Å obtained by Togano *et al.*[10] The peculiarity of the structure is already evident at a basic level: the simple cube cell contains *four* BPd_6 octahedra. This is not possible by simply enlarging the cubic perovskite cell, as its cubic supercells contain 8, 27, ... p^3 octahedra for a $p \times p \times p$ supercell. Thus the *topology* of the BPd_6 octahedra network is distinct from a perovskite such as $MgCNi_3$. This space group consists of a threefold axis without any associated nonprimitive translation; all other rotations are paired with a $(\frac{1}{2}, \frac{1}{2}, 0)$, $(\frac{1}{4}, \frac{1}{4}, \frac{1}{4})$, or $(\frac{3}{4}, \frac{3}{4}, \frac{1}{4})$ type translation. Lack of inversion leaves 24 operations in the point group.

Pd atoms lie at 12*d* sites $(\frac{1}{8}, x_1, \frac{1}{4} - x_1)$ with very low (twofold rotational) symmetry, with reported $x_1 = 0.30417$. Li atoms reside at 8*c* sites (x_2, x_2, x_2) with threefold symmetry, with reported $x_2 = 0.3072$.[13] B atoms within Pd octahedra lie on 4*b* sites $(\frac{5}{8}, \frac{5}{8}, \frac{5}{8})$ and have "32" (threefold+twofold) symmetry. While the B atom lies at the center of mass (CM) of the Pd octahedron and the B-Pd distances are all equal (2.135 Å), the octahedron is strongly distorted. The Pd-B-Pd bond angles are 162° that would be 180° in a cubic perovskite, and the 90° angles become 81°, 89°, and 112°. The distortion keeps one pair of opposing faces of the octahedron perpendicular to the local threefold $< 111 >$ direction.

TABLE I: Significant interatomic distances (in Å) after relaxation. Compared with the experimentally reported value,[13] (↑) and (↓) indicate increase and decrease, respectively. Note that all B-Pd nearest neighbor distances are identical.

Pd−Pd	4×2.779(↓), 2×2.989(↑), 2×3.540(↑)
Pd−B	2×2.135(↑), 1×4.113(↑)
Pd−Li	2×2.693(↓), 2×2.838(↑), 2×3.864(↑)
Li−Li	3×2.584(↓)

The B sublattice consists of symmetry-determined sites, which for the four in the primitive cube lie at $(1,1,1)$, $(-3,3,-1)$, $(-1,-3,3)$, and $(3,-1,-3)$ in units of $\frac{a}{8}$ and with respect to CM of the four. Each B lies on a threefold axis, with B-CM-B angles of 97.6° and 118.3°, so they are not tetrahedrally placed with respect to their CM. This arrangement results in each B atom lying at a connecting vertex of *three* equilateral triangles of B atoms with side length 4.1356 Å. This local connectivity makes the B sublattice resemble a three dimensional generalization of the Kagome lattice, that is, a 3D network of interconnected triangles.

Due to the low xray scattering cross section for Li atoms, the Li position may not have been accurately determined. The two internal parameters mentioned above (Li and Pd) were relaxed within the local density approximation, using the methods discussed below. After relaxation, we obtain for Pd $x_1 = 0.3057$ (different by +0.014 Å) and for Li $x_2 = 0.3018$ (different by −0.063 Å). This difference for Li may be large enough to have significance for the electronic structure. The resulting interatomic distances are given in Table I.

The calculations were done with the full-potential nonorthogonal local-orbital minimum-basis method (FPLO).[20] The fully relativistic scheme,[21] implicitly equivalent to the spin-orbit coupling, implemented in FPLO was also used. Valence bands included Pd $4s4p5s5p4d$, Li $1s2s2p3d$, and B $2s2p3d$. The Brillouin zone was sampled with 200 ($16 \times 16 \times 16$) irreducible k points.

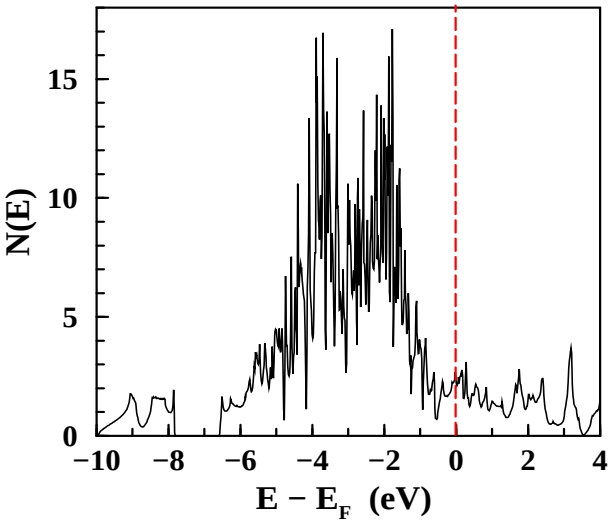


FIG. 1: Total DOS for both spins per a formula unit of Li_2Pd_3B. Every occupied band, except B 2*s* band lying on −10 eV to −8 eV, is strongly mixed above −6.7 eV. But, states from −6 eV to −1 eV are mostly Pd 4*d* states. The vertical dashed line indicates the Fermi energy.

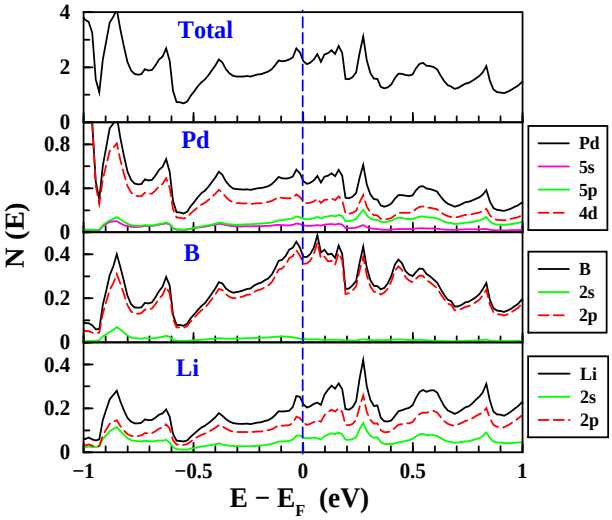


FIG. 2: (Color online)Atomic and orbital projected DOS per atom near the Fermi energy. (The total DOS is given for per eV per formula unit.) $N(0)$ is decomposed into Pd 60%, Li 20%, and B 20%, but in particular Pd 4*d* 50%. Note different scale of $N(E)$ for each plot. The vertical dashed line indicates the Fermi energy.

III. RESULTS AND INTERPRETATION

A. Electronic structure

The density of states (DOS) of the full valence band is given in Fig. 1 and agrees with the result of Chandra et al.[16] B 2*s* states are separate in the −10 eV to −8 eV range. The other occupied bands are a mixture of B 2*p*, Li 2*s* and 2*p*, and Pd 4*d* states. The main complex of Pd 4*d* states extends from −6 to −1 eV, indicating a d^{10} description is most appropriate, but the 4*d* character tails up to 4 eV owing to hybridization with B 2*p* states. The low internal symmetry and twelve Pd atoms per cell lead to 60 Pd 4*d* bands in the 5 eV range, giving rise to the "hairy" DOS in Fig. 1. As a result of the strong hybridization, the B 2*p* states are themselves repelled, so that the B 2*p* states are divided into one region (containing about 20% of the states) from −6.7 eV to −4 eV and another region above −1 eV. The Li 2*p* character is also separated into one region (containing 10% of the states) from −6.7 eV to about −1.3 eV and another region above −1 eV. Separations due to this repulsion make electron-depleted deep valleys, especially around −4 eV and −1 eV. The Li 2*s* states spread across a wide range, but they are only about 20% occupied (i.e. 1/5 and not 1/2 of the isolated Li atom). Thus Li may be somewhat cationic in this compound, a conclusion reached by Chandra *et al.* on geometric grounds.[16]

The band mixture remains complex near the Fermi energy (E_F), as shown by the atomic and orbital projected DOS in Fig. 2 in a small region near E_F (taken as the zero of energy). The total and the Pd contribution are relatively constant within a few tenths of an eV of E_F, whereas the B 2*p* contribution has a maximum near E_F. The DOS at the Fermi level $N(0)$ is 2.24 states/eV per formula unit (both spins).[22] It is composed of 60% Pd, 20% Li, and 20% B characters (note that the contribution *per atom* is almost the same from B as from Pd). In particular, the Pd 4*d* states show the primary contribution, about 50% of $N(0)$, even though the "full *d* bands" are best pictured in terms of a $4d^{10}$ configuration. The linear specific heat coefficient γ = 9.0 mJ/mol-K^2[23] corresponds to a quasiparticle density of states $N^*(0) \equiv (1+\lambda)N(0) = 3.82$ states/eV-formula unit. This leads to a dynamical mass enhancement $\lambda = 0.75$.

The complexity of the band structure is displayed clearly in the expanded band structure near E_F in Fig. 3. Four bands cross E_F, but the most interesting feature comes from as small region of flat bands lying just −70 meV below E_F at both the Γ and X points. The flat bands are sensitive to the position of the atoms, indicative of electron-phonon coupling (see below). In contrast to the result of the previous report[16] using the experimental values of the Li position, the flat bands are located at the identical energy of −70 meV after relaxation, because the flat bands at the Γ and X points have different deformation potentials (Sec. III.D). The difference in

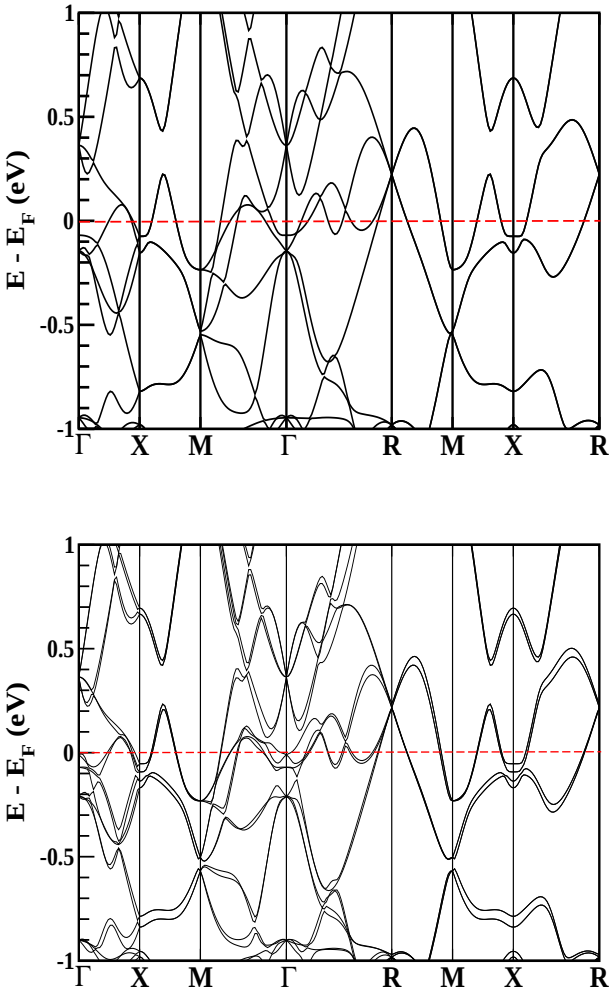


FIG. 3: Blowup of the band structure within 1 eV of the Fermi energy. Note that the flat bands lie at −70 meV at the Γ and X points in the bands without spin-orbit coupling included (top panel). The bottom panel includes spin-orbit coupling (see text for discussion). R denotes the zone boundary point along a < 111 > direction. The horizontal dashed lines indicate the Fermi energy.

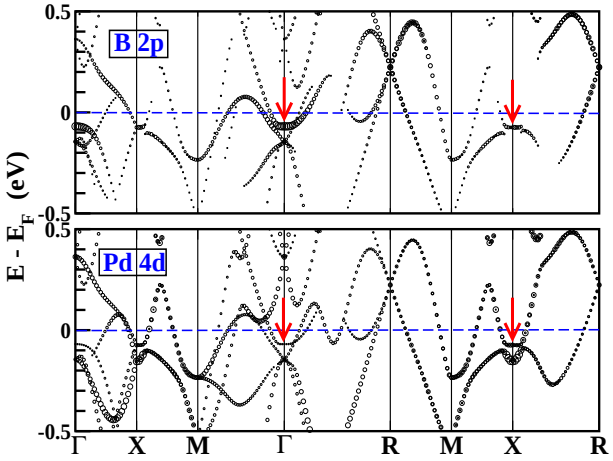


FIG. 4: (Color online)"Fatband" representations of the B $2p$ and Pd $4d$ states within 0.5 eV of the Fermi energy. (Li shows very little character in this range.) The size of symbols is proportional to character of B $2p$ (Pd $4d$) states. The arrows denote the flat bands lying at −70 meV at the Γ and X points. The horizontal dashed lines indicate the Fermi energy.

the deformation potential comes from difference in character of the flat bands, as shown in the fatband representations of Fig. 4. Both flat bands are B $2p$ and Pd $4d$ mixture. However, the band at the Γ point is mostly B $2p$ character, while at the X point Pd $4d$ and B $2p$ characters have similar magnitude.

In addition, the nonsymmorphic space group without inversion leads to unusual behavior in the band structure, as found in MnSi with the B20 structure[8] which also has a cubic Bravais lattice (but a quite distinctive one). The most clearly evident result of the nonsymmorphic nature of this $P4_332$ space group is that it leads to all bands at the zone corner R point being fourfold degenerate, see for example the complex at 0.2 eV in the top panel of Fig. 3. Secondly, many bands at symmetry points have the unusual feature of nonzero velocity due to the space group; see for example the aforementioned bands at the R point, some threefold representations at the Γ point which have two nonzero velocities (at 0.3 eV in the top panel of Fig. 3), and also some bands at the X and M points. This type of "band sticking" due to non-symmorphic operations has been discussed at some length for the case of MnSi.[8] Note that the threefold bands at the Γ point consist of one band with zero velocity and two other bands with nonzero velocities having identical magnitude but opposite sign.

B. Fermi Surfaces

We show the more complex pieces of the Fermi surface in Fig. 5 that correspond to the bands shown in the top panel of Fig. 3. In addition to those shown, there are ellipsoid-like pockets at the X (electron), R (hole), and M (electron) points. The dimensions of these simple pockets can be seen from Fermi level crossings in Fig. 3.

The top panel of Fig. 5 shows a Γ-centered surface that is topologically that of a hollow ball with holes along the cubic axes ("wiffle ball"). The topology of this surface, which encloses holes, is quite involved, with areas of both positive and negative curvature. In addition there are lenses lying along the < 111 > directions; the dimension along the Γ-R line can be obtained from Fig. 3. The bottom panel shows an

electron jack at the Γ point, an additional ellipsoidal surface (holes) at the M point, and a squarish pillow (hole) at the X point.

These Fermi surfaces can be compared with those presented by Chandra *et al.*[16] Although there is much general similarity, there are differences in detail that might have some importance. The wiffle ball and lenses show quite small differences (considering the complexity of this shape). The electron jack has a decidedly different shape but similar size, and one of our ellipsoid-like surfaces around the M point becomes a much more convoluted surface in the result of Chandra *et al.* The associated differences in the two band structures, which can be seen by comparing the band plots, reflect differences in the accuracy of the respective code. They have used a relatively new code VENUS which makes it difficult to speculate on the origin of the differences. We have relaxed the positions of the Li and Pd atoms in our calculation, however, and find that this change makes the extra Γ-centered tiny jack in their calculation disappear in our results.

We have displayed the Fermi surfaces for the bands without spin-orbit coupling. As can be seen from the bottom panel of Fig. 3, the actual Fermi surfaces will be only slightly more complicated due to SOC (see Sec. III C).

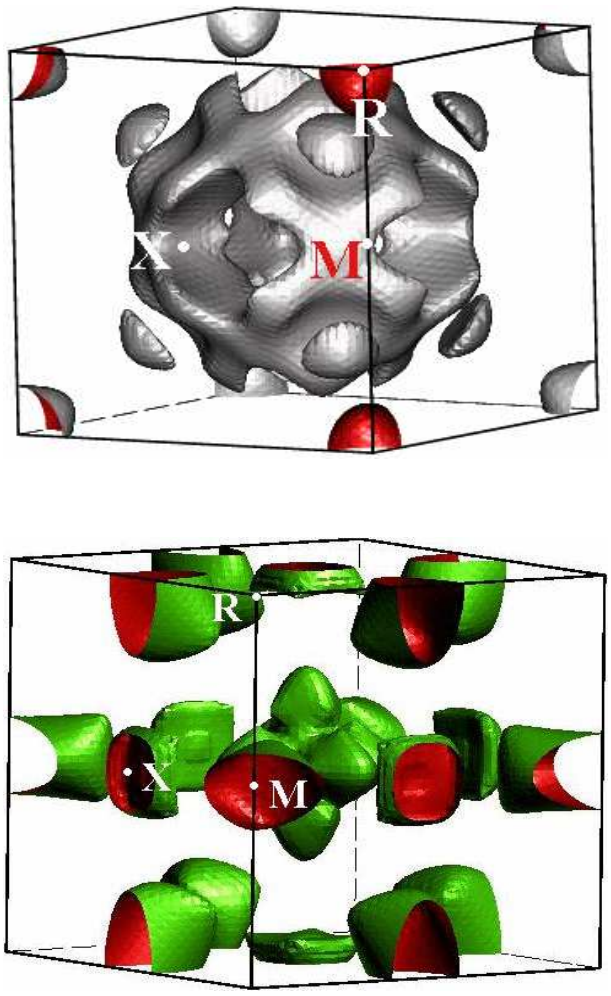


FIG. 5: (Color online) Fermi surfaces of Li_2Pd_3B, with positions of the symmetry points labeled. Several ellipsoid pieces are not shown here, but are noted in the text. The Fermi surfaces shown are from the second and third of the four bands that cross the Fermi energy and are described in the text.

C. Spin-orbit Coupling without Inversion Symmetry

Interest in the effect of SOC in superconductors without inversion symmetry has intensified very recently. Li_2Pd_3B with its $T_c = 8$ K is the prime example at this time: Pd, and more especially Pt, is heavy enough to make SOC an important consideration, and the symmetry deviates seriously from inversion-symmetric. As one example of the magnitude of inversion-breaking: the B-Pd-B bond angle, 180° in a perovskite, is only 162° in this system, and Pd (Pt) is where any appreciable SOC will arise.

The effect of SOC on the band structure of Li_2Pd_3B is displayed in the lower panel of Fig. 3. A surprise is evident: whereas the normal effect of SOC is to lift degeneracies at symmetry points/lines and introduce anticrossings among bands, in this case the number of bands has doubled in addition to the usual effects. This doubling indicates that both spin-up and spin-down bands become mixed and appear on the same band structure, a consequence of the lack of a center of inversion. When inversion symmetry is present, the up- and down-spin bands are still mixed by SOC, but a degeneracy k point by k point is retained, the bands being spin conjugates of each other. It is this degeneracy that the lack of an inversion center removes, and it is the consequences of this lack of symmetry that has attracted attention recently.[2, 3, 4, 5] There is still a degeneracy $\varepsilon_{-k} = \varepsilon_k$ due to time reversal; the first will have mostly spin-up character with some spin-down (say) and the other will the identical amount of spin-down with some spin-up. Lack of inversion does not require exotic pairing, since the states are still time-reversed conjugates and can form singlet pairs (Anderson's theorem). Triplet pairing (or its generalization), on the other hand, is strongly suppressed, being driven to FFLO (Fulde-Farrel-Larkin-Ovchinnikov) type $q \neq 0$ pairing.

Some quantitative estimate of an FFLO modulation in a 'triplet' state can be obtained. Splittings near E_F resulting from SOC + no inversion range

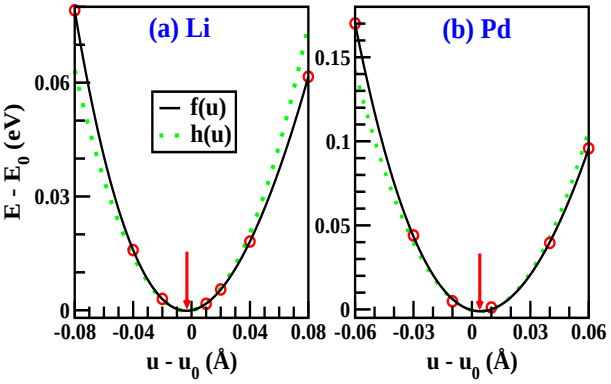


FIG. 6: (Color online)Energy change when (a) Li is displaced along the $<111>$ direction and (b) Pd along the $<011>$ direction. u_0 is the position displaced by -0.06 Å for Li and $+0.01$ Å for Pd from the experimentally reported position. E_0 is energy for u_0. The fitting function f(u) is given by $\varepsilon_0+a_2(u-u_o')^2+a_3(u-u_o')^3+a_4(u-u_o')^4$, and h($u$)=$\varepsilon_0+a_2(u-u_o')^2$ is a harmonic approximated function of f(u). u_o' is the equilibrium position denoted by the vertical arrows.

from zero to 30 meV determined primarily by the amount of Pd character. Given the typical Fermi velocity of 0.75 eV/(π/a)$\approx 3\times10^7$ cm/s, the splitting of Fermi surfaces can be up to $q=\Delta k\sim 0.04\pi/a$, with corresponding modulation wavelength of $\sim 50a$ $\sim$ 350 Å. The cost in kinetic energy is $q^2/2m\sim 1$ meV, which comparing to the superconducting condensation energy $\sim\Delta^2/E_F$ seems to kill any possibility of an FFLO triplet state. Moreover, the observation of a Hebel-Slichter peak in the ^{11}B spin-lattice relaxation time[15] strongly supports nodeless pairing.

D. A_g Phonon Modes

Keeping the space group fixed, we can displace Pd along one $<011>$ direction (its variable internal coordinate) or (and) Li along a $<111>$ direction. Figure 6 shows the energy change for displacement of Li and Pd separately. The data can be fit very well by expanding up to 4th order of the displacement, and the region near the equilibrium position is fit quite well with the harmonic approximation. The fitted constants are given in Table II. By displacing Li and Pd simultaneously, the two A_g phonon frequencies and eigenvectors can be determined. Considering only the harmonic term, the two frequencies are ω_1=40.6 meV (96% from Li and 4% from Pd) and ω_2=13.0 meV (almost 50% from the each type of atom). Clearly ω_2 shows much more coupling effect, 13% softening, whereas ω_1 has nearly negligible coupling, consistent with the character of the phonon eigenvectors. The value of ω_1 is almost exactly equal to the experimentally reported maximum value of Li metal,[24] whereas ω_2 is much softer than the 30 meV maximum for Pd metal.[25]

TABLE II: Fitting parameters of the energy change for Li and Pd displacements. The parameters, a_n for Li and b_n for Pd (in eV/Å^n), are coefficients of the nth order displacement terms and c (in eV/Å^2) is the first order coupling term. The frequency ω obtained from the harmonic approximation is given in meV. Li/Pd denotes a case where both atoms were displaced. The force constant $m\omega^2$, where m is an atomic mass, is 2.7 for Li and 5.8 for Pd (in eV/Å^2).

displaced atom	a_2, b_2	a_3, b_3	a_4, b_4	c	ω
Li $<111>$	10.8	−29.6	73.5		40.4
Pd $<011>$	34.7	−83.6	357.5		15.0
Li/Pd	10.6	−32.1	151.8		40.6
	33.2	−94.4	583.0	16.9	13.0

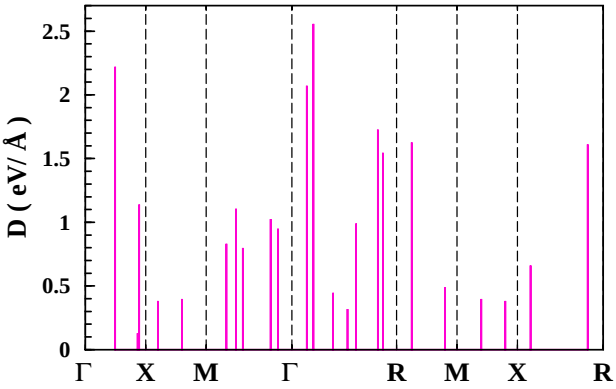


FIG. 7: (Color online)Distribution of the deformation potential $\mathcal{D}$ at the Fermi level, when Pd moves along the $<011>$ direction. The vertical bar indicates the strength, and is placed at the positions where the bands cross the Fermi level.

E. Deformation Potential

A deformation potential $\mathcal{D}$ is defined as an energy shift with respect to (periodic) atomic displacement. Figure 7 displays the strong k variation of the deformation potential for selected bands at E_F with respect to Pd motion along the $<011>$ direction. The value is large near the Γ and R points but smaller near the M and X points, reflecting the strong variation of the Pd character around the Fermi surface. The variation of Pd/B character is pictured in the fatband representations given in Fig. 4, but the deformation potential may not be simply related to the amount of Pd character. The averaged potential

$\langle \mathcal{D}_{\mathtt{Pd}} \rangle$ for these points, and its variance, is 1.15(±0.6) eV/Å, a value indicating significant Pd contribution to electron-phonon coupling, as we show below. The maximum value of about 4 eV/Å=3.4 $\langle \mathcal{D}_{\mathtt{Pd}} \rangle$ occurs for the flat band lying just below E_F at the Γ point (not shown in Fig. 7), whereas the other flat band at the X point has a value only comparable with $\langle \mathcal{D}_{\mathtt{Pd}} \rangle$.

For a physical feeling for the magnitude of the coupling, note that the flat band at the Γ point with large deformation potential crosses E_F when Pd is displaced by about −0.03 Å , while at the X point it requires a displacement of −0.06 Å from the relaxed position. B $2p$ character at E_F is consistent with the ^{11}B NMR data of Nishiyama and coworkers.[15] Unlike Pd, the Li deformation potential is small (by an order of magnitude) $\langle \mathcal{D}_{\mathtt{Li}} \rangle$= 0.11(±0.06) eV/Å, with the maximum value of 0.27 eV/Å occurring at the Γ point. The contribution of the deformation potentials to the electron-phonon coupling constant can be measured by the quantity Λ_i=N(0)$\langle \mathcal{D}_i^2 \rangle / \langle M_i \rangle \omega_i^2$, where $\langle M_i \rangle$ is an average mass of mode i (for example, approximately $M_{\mathtt{Li}}$ for ω_1 and a half of $M_{\mathtt{Pd}}$+$M_{\mathtt{Li}}$ for ω_2). Using the mean of the two values of $\langle \mathcal{D}_2 \rangle$ for Λ_2, the ratio of Λ_2/Λ_1 is 30, clearly indicating that the electron-phonon coupling is mainly from Pd contribution. We have however not assessed possible coupling from the B atom. The large C isotope coefficient[26] $\alpha_C = 0.54$ in $MgCNi_3$ suggests that coupling to B indeed may be important.

We have used the Allen-Dynes equation[27] to assess these quantities in relation to the measured T_c = 8 K. Clear conclusions are not possible because for T_c of 8 K or less, the uncertain value of the effective Coulomb repulsion μ^* introduces uncertainty. We concentrate on the value $\lambda \sim 0.7$, which is the specific heat mass enhancement, and this value is also the "mode λ" for the lower frequency A_g mode. Using a representative phonon frequency Ω = 13 meV (the A_g mode), then $\mu^* = 0.10$ gives T_c = 5.4 K, while μ^*=0.15 gives T_c = 3.7 K. Increasing Ω to 23 meV, the values become $T_c(\mu^*=0.10)$ = 9.6 K, $T_c(\mu^*=0.15)$ = 6.0 K. These values indicate that a mean phonon energy of 20 meV with λ = 0.7 may be necessary to account for T_c^{exp} = 8 K.

IV. THE Pt ANALOG

The decrease of T_c from 8 K to less than 3 K in the Pt analog provides a potentially important clue into the mechanism of superconductivity, so we have looked at the differences in the electronic structure. For Li_2Pt_3B, we used the experimentally reported structure without relaxation,[13] since relaxation produced relatively small difference in

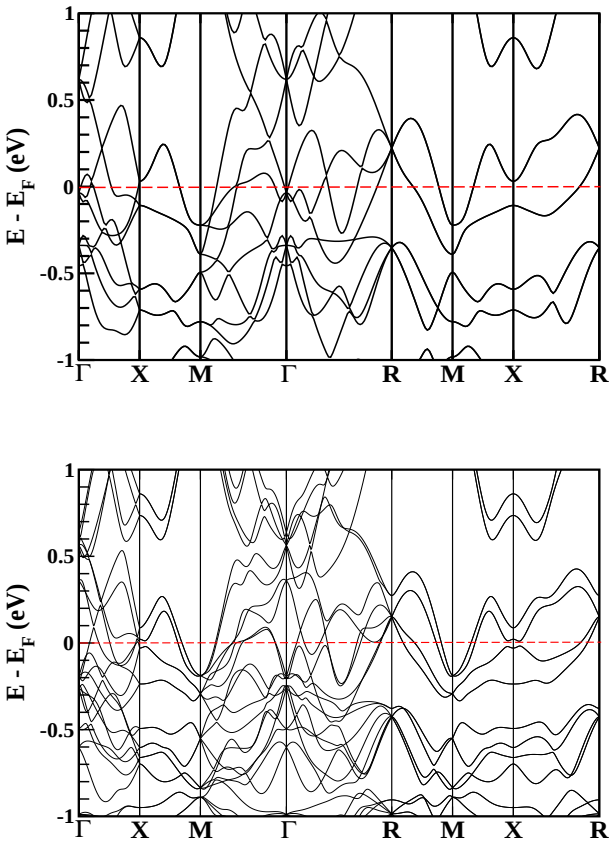


FIG. 8: Blowup of the Li_2Pt_3B band structure within 1 eV of the Fermi energy, plotted identically to those for Li_2Pd_3B in Fig. 3. Top panel, without spin-orbit coupling; bottom panel, spin-orbit included. Even without spin-orbit, it is rather difficult to see any close correspondence between the Li_2Pt_3B and Li_2Pd_3B (Fig. 3) bands; see text for further discussion of differences. The bottom panel reveals the strong effects in Pt arising from coupling of the spins to real space motion of electrons.

Li_2Pd_3B. The valence orbitals of Pt were taken to be $4f5s5p6s6p5d$, with Li and B being treated as before.

The resulting band structure is plotted in Fig. 8 on the same scale as those of Li_2Pd_3B in Fig. 3, so direct comparison can be made. Given the same cell volume and the similarity of Pd and Pt in many respects, it is somewhat surprising that the bands show so much difference. The Fermi level DOS actually increases, to 2.9 states/eV per formula unit. The differences, such as more bands in the region within 1 eV below E_F, can be traced to the wider bandwidth, which also places more d character at E_F. The occupied bandwidth is 7.6 eV compared to 6.7 eV in Li_2Pd_2B (Fig. 1) and the d bandwidth (region of large DOS) is ∼15% wider and extends more strongly to E_F.

The bottom panel of Fig. 8 shows the consequence

of SOC in the Pt compound. Splittings near E_F as large as 200 meV occur, for example, the band below E_F at the X point. More generally, the splittings are perhaps on average a factor of two or so larger than for the Pd compound. It can be seen that fourfold degeneracies at the R point survive SOC, as do the degeneracies at the M point, while the threefold states at the Γ point are split to doublet plus singlet.

The FPLO method, being atomic orbital based, can be used to provide a Mulliken decomposition of charges. While the atomic charges depend somewhat on the choice of orbitals, it is possible that the differences in charges for these two compounds can provide some insight. The Mulliken effective charges are, in the Li_2Pd_3B compound: Li, −0.08; Pd, +0.17; B, −0.34; and for the Li_2Pt_3B compound: Li, +0.11; Pt, +0.02; B, −0.28. The main difference is that Pt is effectively neutral while Pd is noticeably cationic. These charges do not support the suggestions, discussed earlier, that Li is cationic in Li_2Pd_3B, although it may become somewhat anionic in Li_2Pt_3B.

V. DISCUSSION AND SUMMARY

Considering that the local coordination and the similar valences of the constituents (Li_2 ↔ Mg, Pd ↔ Ni, B with one less electron than C) and that both compounds superconduct at the same temperature of 8 K, it is worthwhile to consider whether there is any realistic comparison with $MgCNi_3$. In both systems there is a nominal d^{10} configuration of the transition metal atom, but strong d character remains at the Fermi surface. The volume per formula unit is 30% larger in Li_2Pd_3B, much more than expected from simple Ni→Pd replacement and reflecting the more open structure of Li_2Pd_3B. Moreover, the band structures do not show much resemblance (the four times larger cell makes comparison difficult, however). The DOS of $MgCNi_3$ is dominated by a very high and very narrow peak in the density of states 45 meV below E_F, derived from a very flat band all around the M point of the Brillouin zone. In Li_2Pd_3B there is no analogous feature (see Fig. 3). There is a fairly flat band along the M-X line that is cut, and hybridized with, a steeper band, as can be seen in Fig. 4, but there is no corresponding DOS peak. The value of N(0) is only 45% of that of $MgCNi_3$ (per formula unit).[28] The band filling is, of course, one electron higher in Li_2Pd_3B.

Generally, we identify no close relationship between the electronic structures of these two systems, and the differences are substantial. The lack of inversion symmetry and substantial (large) spin-orbit coupling in the Pd (respectively, Pt) compound make the electronic structure much richer, with complicated Fermi surfaces. Comparison of the calculated N(0) with the linear specific heat coefficient leads to a dynamical mass enhancement $\lambda \sim 0.75$, which if due to electron-phonon coupling is in the right range to account for T_c. One particular Pd vibration is calculated to have a mode λ of this same size. However, the Li A_g mode is found to be very weakly coupled. This means that the electron-phonon coupling varies strongly throughout the phonon spectrum, and most likely also across the Fermi surface.

The differences between Li_2Pd_3B and Li_2Pt_3B are strong enough that the origin of the difference in their values of T_c is unclear. Strong spin-orbit coupling together with the lack of inversion symmetry, coupled with the observation of a Hebel-Slichter coherence peak in the spin-lattice relaxation rate, strongly points to conventional rather than exotic pairing, and we have begun to probe electron-phonon coupling in this system. $MgCNi_3$ has been found to have very strong coupling to certain modes,[29] if the analogy to this compound is relevant. If the coupling is primarily to the Pd (Pt), the difference in masses leads to a decrease by $\sqrt{106/195} = 0.74$, roughly half of the reduction factor that is needed. A difference in λ of only 15% would be required to give the further reduction of T_c, and the electronic structure is different enough to allow this possibility.

VI. ACKNOWLEDGMENTS

We thank K. Togano and H. Takeya for communicating experimental results on the linear specific heat coefficient prior to publication. Discussions with A. B. Shick about implications of lack of inversion symmetry have been very helpful. This work was supported by National Science Foundation grant No. DMR-0421810.

[1] E. Bauer, G. Hilscher, H. Michor, Ch. Paul, E. W. Scheidt, A. Gribanov, Yu. Seropegin, H. Noël, M. Sigrist, and P. Rogl, Phys. Rev. Lett. **92**, 027003 (2004).

[2] K. V. Samokhin, E. S. Zijlstra, and S. K. Bose, Phys. Rev. B **69**, 094514 (2004).

[3] I. A. Sergienko and S. H. Curnoe, Phys. Rev. B **70**, 214510 (2004).
[4] K. V. Samokhin, Phys. Rev. Lett. **94**, 027004 (2005).
[5] P. A. Frigeri, D. F. Agterberg, and M. Sigrist, New J. Phys. **6**, 115 (2004).
[6] C. Pfleiderer, G. J. McMullan, S. R. Julian, and G. G. Lonzarich, Phys. Rev. B **55**, 8330 (1997).
[7] P. A. Frigeri, D. F. Agterberg, A. Koga, and M. Sigrist, Phys. Rev. Lett. **92**, 097001 (2004).
[8] T. Jeong and W. E. Pickett, Phys. Rev. B **70**, 075114 (2004).
[9] T. Akazawa, H. Hidaka, T. Fujiwara, T. C. Kobayashi, E. Yamamoto, Y. Haga, R. Settai, and Y. Onuki, J. Phys.: Condens. Matter **16**, L29 (2004).
[10] K. Togano, P. Badica, Y. Nakamori, S. Orimo, H. Takeya, and K. Hirata, Phys. Rev. Lett. **93**, 247004 (2004).
[11] P. Badica, T. Kondo, T. Kudo, Y. Nakamori, S. Orimo, and K. Togano, Appl. Phys. Lett. **85**, 4433 (2004).
[12] M. Saradar and D. Sa, Physica C **411**, 120 (2004). Results of this paper appear to arise from an incorrect understanding of the crystal structure.
[13] U. Eibenstein and W. Jung, J. Solid State Chem. **133**, 21 (1997).
[14] T. Yokoya, T. Muro, I. Hase, H. Takeya, K. Hirata, and K. Togano, Phys. Rev. B **71**, 092507 (2005).
[15] M. Nishiyama, Y. Inada, and G.-Q. Zheng, Phys. Rev. B **71**, 220505(R) (2005).
[16] S. Chandra, S. Mathi Jaya, and M. C. Valsakumar, cond-mat/0502525.
[17] P. Badica, T. Kondo, and K. Togano, J. Phys. Soc. Jpn. **74**, 1014 (2005).
[18] T. He, Q. Huang, A. P. Ramirez, Y. Wang, K. A. Regan, N. Rogado, M. A. Hayward, M. K. Haas, J. S. Slusky, K. Inumara, H. W. Zandbergen, N. P. Ong, and R. J. Cava, Nature **411**, 54 (2001).
[19] R. E. Schaak, M. Avdeev, W.-L. Lee, G. Lawes, H. W. Zandbergen, J. D. Jorgensen, N. P. Ong, A. P. Ramirez, and R. J. Cava, J. Solid State Chem. **177**, 1244 (2004).
[20] K. Koepernik and H. Eschrig, Phys. Rev. B **59**, 1743 (1999).
[21] H. Eschrig, M. Richter, and I. Opahle, in *Relativistic Electronic Structure Theory - Part II: Applications*, edited by P. Schwerdtfeger (Elsevier, Amsterdam, 2004), pp. 723-776.
[22] Relaxation of the atomic position decreased the value of N(0) by 4%. Using the experimentally reported atomic position[13] and 140 irreducible k points as was done in Ref. [14], we obtained the same value they reported.
[23] H. Takeya, K. Yamada, K. Yamaura, T. Mochiku, H. Fujii, T. Furubayashi, K. Hirata and K. Togano (private communication); Physica C (in press).
[24] V. Bortolani and G. Pizzichini, Phys. Rev. Lett. **22**, 840 (1969), and references therein.
[25] A. P. Miller and B. N. Brockhouse, Phys. Rev. Lett. **20**, 798 (1968).
[26] T. Klimczuk and R. J. Cava, Phys. Rev. B **70**, 212514 (2004).
[27] P. B. Allen and R. C. Dynes, Phys. Rev. B **12**, 905 (1975).
[28] M. D. Johannes and W. E. Pickett, Phys. Rev. B **70**, 060507(R) (2004).
[29] A. Yu. Ignatov, S. Y. Savrasov, and T. A. Tyson, Phys. Rev. B **68**, 220504(R) (2003).